RSC Advances

PAPER

Cite this: *RSC Adv.*, 2016, **6**, 21929

# Efficient removal of rhodamine 6G dye from aqueous solution using nickel sulphide incorporated polyacrylamide grafted gum karaya bionanocomposite hydrogel†

Neeraj Kumar,[a] Hemant Mittal,[ab] Vyom Parashar,[a] Suprakas Sinha Ray[ab] and Jane Catherine Ngila*[a]

Received 17th November 2015
Accepted 9th February 2016

DOI: 10.1039/c5ra24299a

www.rsc.org/advances

This research paper reports the synthesis and usage of the polyacrylamide (PAAm) grafted gum karaya (Gk) and nickel sulphide nanoparticle based hydrogel to effectively remove rhodamine 6G dye (R6G) from aqueous solution. Initially, the hydrogel polymer of the Gk with the PAAm was synthesized using the graft co-polymerization technique. In the second step, the nickel sulphide nanoparticles were incorporated *in situ* within the hydrogel polymer matrix. The synthesized hydrogel nanocomposite was characterized using different characterization techniques such as XRD, FTIR, SEM, and TEM. The changes in the surface area, pore volume and pore diameter after the incorporation of nanoparticles were studied using the BET technique. The adsorption of R6G onto the hydrogel nanocomposite followed the Langmuir adsorption isotherm with a maximum adsorption capacity of 1244.71 mg $g^{-1}$. The adsorption kinetics followed the pseudo-second order rate model. Furthermore, various thermodynamic parameters such as $\Delta S^\circ$, $\Delta H^\circ$ and $\Delta G^\circ$ were calculated to check the spontaneity and nature of the process of adsorption. The hydrogel nanocomposite was used for five successive cycles of adsorption–desorption. Therefore, the nanocomposite hydrogels have proved their potential for the removal of cationic dyes from aqueous solutions.

## 1 Introduction

Since antiquity, dye has been an integral part of human civilization in art, textiles, plastic and current technologies. Chemicals that are involved in synthetic dye production are toxic, carcinogenic and sometimes explosive.[1] Almost every industry uses water-soluble dye and discards these dye effluents directly into the environmental water system (mostly fresh water).[2] It is estimated that over $7 \times 10^5$ tons of synthetic dyes are annually produced worldwide, up to 200 000 tons of which are released into the environment as effluents every year.[3,4] This practice is a deadly risk to both the environment[5,6] and to human health.[7] The reason for this huge amount of discarded dyes is the inefficiency of the available dyeing process. Different techniques such as photocatalysis, adsorption, coagulation–flocculation, advanced oxidation processes, ozonation, membrane filtration, ion exchange and biological degradation have been developed and implemented to remove dye pollutants from waste water.[8,9] Most of these techniques have serious drawbacks such as the generation of a huge amount of by-products, incomplete dye removal, high reagent and energy necessity, high operational cost and low selectivity. Among various available techniques adsorption is suggested as one of the most promising methods because of its simplicity and effectiveness.[10,11]

In this context, polymers have emerged as the most alluring class of adsorbents among which natural polymers (*e.g.* polysaccharides) gain special attention because of their environment-friendly nature.[12–15] In this regard, one focus area in natural polymers is to increase their adsorption and regeneration capacity.[13,16] To attain these goals researchers have turned their attention towards nanomaterials to exploit their size-dependent properties, which provide access to better adsorption kinetics.[11] The amalgamation of nanomaterials ($SiO_2$, $TiO_2$, $Fe_2O_3$, $Fe_3O_4$, CdSe and Ag) and natural polymers (particularly polysaccharides such as pectin, starch, guar gum, gum ghatti, and gum xanthan) has shown great promises to combat the conundrum of toxic effluents in water.[17–26] In our previous work we explored the $Fe_3O_4$–graphene nanocomposite for arsenic removal[27] and our results motivated us to further work on metal sulphides nanoparticles with natural polysaccharides polymers to address the dye-related pollution.

[a]*Department of Applied Chemistry, University of Johannesburg, Doornfontein 2028, South Africa. E-mail: jcngila@uj.ac.za*

[b]*DST/CSIR National Centre for Nanostructured Materials, Council for Scientific and Industrial Research, Pretoria 0001, South Africa*

† Electronic supplementary information (ESI) available: Table contains optimization of different grafting parameters for the synthesis of BioNC hydrogel nanocomposites and isotherms, kinetics and thermodynamics studies results. See DOI: 10.1039/c5ra24299a

In the present work, we have elected nickel sulphide and polysaccharide gum karaya (Gk) to develop a high dye adsorption bionanocomposite (BioNC) hydrogel. Nickel sulphide was an obvious ideal choice because of its excellent catalytic behaviour[28] and environment friendly nature whereas the choice of Gk was predominantly considered because of its excellent physiochemical properties, occurrence and easy production.[29,30] Moreover, nickel sulphide nanoparticles were selected to investigate their role in the adsorption kinetics compared to oxide nanomaterials explored in previous studies.[11,17,23] Further, the excessive surface functionality of Gk with nickel sulphide nanoparticles fabricate a new adsorbent to remove pollutants from water. We selected rhodamine 6G (R6G) a cationic rhodamine family dye as a model system to investigate the efficiency of the fabricated BioNC hydrogel. In addition, this work also addresses a facile new route to synthesize nickel sulphide nanoparticles using eco-friendly additive SHMP (sodium hexametaphosphate) at low temperature.

## 2 Experimental sections

### Chemicals and reagents

Gk, acrylamide (AAm), potassium persulphate (KPS), ascorbic acid (ABC), *N*,*N*′-methylene-bis-acrylamide (MBA), R6G, nickel(II) acetate tetrahydrate, sulphur powder and sodium hexametaphosphate (SHMP) were purchased from Sigma Aldrich, South Africa and used without further purification. All other chemical were of analytical grade and used as received. Deionized water was used for all experiments.

### Synthesis of nickel sulphide nanoparticles ($NiS/Ni_3S_4$ NPs)

The nickel sulphide nanoparticles were made in solution using the ionic starting materials nickel acetate tetrahydrate ($Ni(CH_3CO_2)_2\cdot 4H_2O$) and elemental sulphur in the presence of HMP. In this procedure, $Ni(CH_3CO_2)_2\cdot 4H_2O$ was dissolved in water to a concentration of 0.1 M. After stirring for 15 min, 25 mM of HMP was added and the solution was continuous stirred for 15 min at 70 °C. Then, 0.1 M sulphur solution (reduced by 1 mL of hydrazine hydrate) was added drop-wise and the final reaction mixture was stirred for 2.5 h with continuous heating at 120 °C. The obtained black colour precipitations were centrifuged three times with deionized water and finally with ethanol at 7000 rpm to remove unreacted chemicals; then they were dried at 60 °C for 5 h.

### Synthesis of the Gk-cl-PAAm hydrogel

In the first step, the hydrogel polymer of AAm onto Gk was synthesized using ABC–KPS as the redox initiator and MBA as a crosslinking agent through the free-radical graft co-polymerization technique. To better disperse the Gk in water, Gk (1 g) was initially added to 20 mL of deionized water in a 100 mL glass beaker and kept undisturbed for 24 h. Then, a definite ratio of KPS and ABC (Table S1, ESI†) was added into reaction mixture and vigorously stirred; the required amount of the crosslinker, *i.e.*, MBA was subsequently added into reaction mixture with continuous stirring. In the last step of this reaction, particular amounts of monomer, *i.e.*, AAm were added in the reaction mixture (Table S1, ESI†) and the reaction was allowed to proceed without disturbance. After the desired time interval, the reaction was stopped and allowed to cool at room temperature. The unreacted reactants were separated by the Soxhlet extraction with acetone. The synthesized hydrogel polymer *i.e.* Gk-cl-PAAm was dried in a hot-air oven at 50 °C for 12 h. The dried hydrogel samples were pulverized in a ball mill. The hydrogel polymer sample to synthesize the nanocomposite was selected based on maximum percentage swelling ($P_s$), which was calculated as follows:

$$\text{Percentage swelling} = \frac{W_f - W_i}{W_f} \times 100 \quad (1)$$

where, $W_f$ is the weight of the hydrogel polymer after swelling and $W_i$ is the weight of the dried hydrogel polymer sample. Different optimized graft co-polymerization parameters are listed in Table S1, ESI.†

### Synthesis of the BioNC hydrogel

To synthesize the BioNC hydrogel, the hydrogel polymer, *i.e.*, Gk-cl-PAAm, which was synthesized in the first step, was used as the polymer matrix and the $NiS/Ni_3S_4$ NPs were used as the filler. Initially, various amounts of $NiS/Ni_3S_4$ NPs were introduced into 20 mL deionized water and sonicated for 2 h. After the NPs were homogeneously dispersed, 1 g Gk was added into reaction mixture and thoroughly stirred. Then, the graft co-polymerization reaction was performed with the optimized reaction parameters in the first step. The best hydrogel polymer for the remainder of studies was selected based on percentage swelling ($P_s$), which was calculated using eqn (1) (Table S1, ESI†). Because the sample BioNC hydrogel-3 showed the highest $P_s$ value, it was used for present studies. The BioNC hydrogel-3 is denoted as BioNC hydrogel in the entire article to avoid the reader's confusion. Various steps in the synthesis mechanism of the BioNC hydrogel are depicted in Scheme 1.

### Characterization

The structural composition, morphological features and physiochemical properties of the parental polymer matrix *i.e.* Gk-cl-PAAm and the BioNC hydrogel were studied using different characterization techniques. The powder X-ray diffraction (XRD) analysis of the samples was performed out with a PANalytical X'Pert PRO X-ray diffractometer using Cu K$\alpha$ radiation with a wavelength of 1.5406 Å and visible light at 40 kV/40 mA. FT-IR spectra were recorded in the solid state (KBr pellet method) using a Perkin-Elmer Spectrum 100 spectrometer in the spectral range of 4000–400 $cm^{-1}$ with a resolution of 4 $cm^{-1}$ for the structural determination, confirmation of the grafting of PAAm onto Gk and the successful incorporation of $NiS/Ni_3S_4$ NPs in the polymer matrix. The particle sizes and morphology of synthesized $NiS/Ni_3S_4$ NPs and morphological change of Gk, which occurred through the graft co-polymerisation and further incorporation of $NiS/Ni_3S_4$ NPs within the polymer network of Gk-cl-PAAm hydrogel were studied using field emission scanning electron microscopy (TESCAN, VEGA SEM) under a 20 kV

 

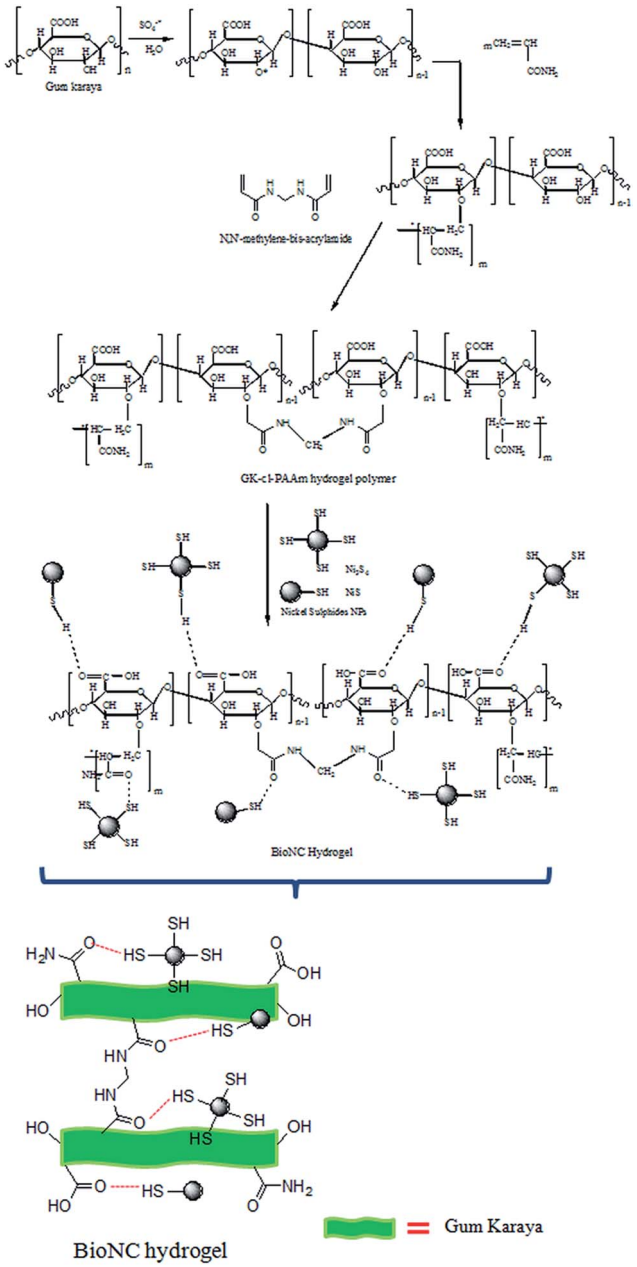


Scheme 1 Best possible proposed mechanism to synthesize the BioNC hydrogel.

electron acceleration voltage which was coupled with an energy dispersive X-ray spectroscope (EDS) and JEOL JEM-2100F (TEM) with an accelerating voltage of 90 kV. The specific Brunauer–Emmett–Teller (BET) surface areas and pore-size distributions of the parent hydrogel polymer matrix and BioNC hydrogel were studied using nitrogen adsorption–desorption measurements on a Micromeritics, ASAP 2020, surface area and porosity analyzer. The samples were degassed at 150 °C overnight before the measurements. To determine the point of zero charge (pzc), 0.2 g of the BioNC hydrogel was added in the solutions of different pH in the range of 2.0–11.0 and the solutions were periodically shake over a water bath until the pH value stabilised. The difference between the final and initial pH was termed as ΔpH and it was plotted against the initial pH to determine the pzc.[31] The concentration of the free oxygen functional groups, such as –OH and –COOH, on the BioNC hydrogel was determined using the Boehm titration.[13] The BioNC hydrogel was dried in a hot air oven for 24 h. 0.5 g of the BioNC hydrogel was added in 25 mL of the alkali solutions (0.1 N NaOH and 0.1 N $NaHCO_3$) separately. The samples were stirred at 25 °C for 4 h. After that the 5 mL of the supernatant was taken and back titrated against 0.1 N HCl solutions. The concentrations of different functional groups present in the BioNC hydrogel were determined by the residual bases after back titration.

### Adsorption study experiments

The adsorption experiment of an aqueous solution of R6G was performed using a thermostatic water-bath shaker at 20 °C and 120 rpm for 24 h in 100 mL glass bottles. Different adsorption parameters such as the solution pH and amount of adsorbent dose for the maximum adsorption of R6G using BioNC hydrogel were optimized in batch mode. The effect of solution pH on the adsorption of R6G was studied over the pH range of 2.0–11.0 and the pH of different solutions was adjusted using 0.1 M NaOH and 0.1 M HCl solutions. For all batch experiments, 0.4 g $L^{-1}$ of the BioNC hydrogel was introduced into 50 mL dye solution (50 mg $L^{-1}$) in glass bottles, which were shaken for 24 h. After the desired time interval, the sample bottles were taken out of the thermostatic water-bath shaker and the suspensions were filtered using 0.45 μm PVDF syringe filters. A UV-Vis spectrometer (Shimazdu, UV-2450, UV-Vis spectrophotometer, Japan) was used to analyses the concentration of unabsorbed dye after adsorption at 525 nm as $\lambda_{max}$ of R6G.[32] The adsorption efficiency or percentage adsorption of the dye was calculated as follows:[20]

$$\text{Percentage removal} = \frac{C_o - C_e}{C_o} \times 100 \quad (2)$$

where, $C_o$ is the initial concentration of R6G (mg $L^{-1}$) and $C_e$ is the equilibrium concentration (mg $L^{-1}$) of unadsorbed R6G remained in the solution.

After the pH optimization, the effect of BioNC hydrogel dose on the adsorption capacity was studied by varying the amount from 0.1–1.0 g $L^{-1}$ at pre-optimized solution pH under the adsorption conditions to those that were used to optimize the solution pH and the adsorption percentage was calculated using eqn (2). The adsorption isotherm studies were performed at different temperature (25, 35 and 45 °C) for 24 h at pre-optimized pH and BioNC hydrogel dose using 50 mL dye solutions of different concentrations, which varied in the range of 50–500 mg $L^{-1}$. The equilibrium adsorption ($q_e$) was calculated using following equation:[20]

$$q_e = \frac{C_o - C_e}{m} \times V \quad (3)$$

where, $q_e$ is the equilibrium adsorption of dye per unit mass of adsorbent (mg $g^{-1}$), $m$ is the mass of adsorbent (g) and $V$ is the volume of dye taken (L).

Adsorption kinetics experiments were conducted on a mechanical stirrer with a shaking speed of 100 rpm at 25 °C using with three different initial dye concentrations (50, 75 and 100 mg $L^{-1}$). Then, 0.4 g of BioNC hydrogel was introduced into 1000 mL of dye solution and agitated for various time intervals in the range of 0–4 h. At regular time intervals 5 mL of sample aliquot was collected and filtered, and the concentration of unadsorbed R6G was determined as earlier.

The amount of R6G adsorbed at different time intervals was calculated using the following equation:[13]

$$q_t = \frac{C_o - C_t}{m} \times V \quad (4)$$

where, $q_t$ is the amount of dye adsorbed per unit mass of the adsorbent (mg $g^{-1}$) at time $t$ and $C_t$ denotes the concentration of dye (mg $L^{-1}$) at time $t$ that remained in the solution.

### Adsorption from simulated wastewater

The adsorption capacity of BioNC hydrogel was also checked with respect to the removal of pollutants from synthetic wastewater. Multiple dye solutions comprising mixtures of cationic dyes *viz.* methylene blue (MB), R6G, and brilliant green (BG) and an anionic dye Congo red (CR) at individual concentration of 12.5 mg $L^{-1}$ were prepared in 1 M NaCl (50 mL). Various amounts of adsorbent were added to the synthetic wastewater and the effect of the mass of the adsorbent on the percentage adsorption of each dye in the solution was studied.

### Desorption and reusability experiments

The regeneration ability of the BioNC hydrogel to remove R6G was studied for 5 subsequent adsorption–desorption cycles using the optimum adsorption conditions such as pH (7.0) and adsorbent dose (0.4 g $L^{-1}$). In each cycle, 0.4 g $L^{-1}$ of BioNC hydrogel was added in 50 mg $L^{-1}$ dye solution and shaken for 24 h. Dye-loaded particles of BioNC hydrogel were separated from the dye solution, dried and added into 50 mL of 0.1 M HCl solution and shaken for 24 h. After each cycle, the desorbed samples of BioNC hydrogel were washed with water, dried, weighed and recycled using 0.1 M HCl and again used for the adsorption of R6G in the next cycle. The process was used for five successive cycles of adsorption–desorption of R6G. The percentage desorption was calculated by using the following equation:

$$\%\ \text{desorption} = \frac{\text{concentration desorbed (mg } L^{-1})}{\text{concentration adsorbed (mg } L^{-1})} \times 100 \quad (5)$$

## 3 Results & discussion

### Characterization of the BioNC hydrogel

Different characterization tools such as XRD, FT-IR, TEM, SEM-EDX and BET were used to confirm the successful formation of the BioNC hydrogel and incorporation and uniform distribution of NiS/$Ni_3S_4$ NPs in the cross-linked polymer matrix of Gk-cl-PAAm hydrogel.

The crystalline structure of synthesized NiS/$Ni_3S_4$ NPs and their BioNC hydrogel were first analysed using a powder XRD technique. Fig. 1d shows the XRD patterns of pure NiS/$Ni_3S_4$ NPs and nanocomposites. All diffraction peaks were well indexed, and both position and intensity of the diffraction peaks were well matched to those of the standard card of $Ni_3S_4$ (JCPDS No. 47-1739) and NiS (JCPDS No. 02-1273). It is clearly noticed that the $Ni_3S_4$ phase has higher intensity than NiS, which indicates a higher percentage of $Ni_3S_4$ in the sample. The XRD pattern of BioNC hydrogel exhibit the amorphous nature and characteristic peaks at 11.7, and 20.8 at 2$\theta$ scale exhibit the graft polymerization of Gk with acrylamide (Gk-cl-PAAm).[33] Furthermore, the successful incorporation and uniform distribution of NiS/$Ni_3S_4$ NPs into the Gk-cl-PAAm matrix were confirmed by the presence of major characteristic peaks at 2$\theta$ 29.1, 30.46, 31.4, 34.9, 46.2 and 53.7 with reduced intensity.

The composition of the BioNC hydrogel and NiS/$Ni_3S_4$ NPs was studied using FT-IR, as shown in Fig. 1e. For nickel sulphides, the characteristic peak of Ni–S appears at 982 $cm^{-1}$.[34] In the BioNC hydrogel spectrum, the peaks at 3349 $cm^{-1}$ implies the existence of hydroxyl groups (–OH), and the signals at 2965 $cm^{-1}$ and 2846 $cm^{-1}$ are related to aliphatic (–$CH_2$) stretching vibrations. The peaks at 1710 $cm^{-1}$ and 1650 $cm^{-1}$ are ascribed to the stretching vibration of –COOH and –$CONH_2$ in the BioNC hydrogel spectrum, respectively. Further, a series of peaks appeared at 1455 $cm^{-1}$, because of the amide –NH in-plane bending; 1232 $cm^{-1}$, because of the amide –CN stretching vibration; and 778 $cm^{-1}$, because of the amide –OCN deformation. The absorption peak at 1047 $cm^{-1}$ is attributed to the pyranose rings of the polysaccharides. The nickel sulphides peaks at 982 $cm^{-1}$ merged into previous peaks of the BioNC hydrogel. Therefore, the presence of characteristic peaks of Gk-cl-PAAm matrix and NiS/$Ni_3S_4$ NPs in the spectrum of the BioNC hydrogel confirms the successful grafting and, incorporation and uniform distribution of nanoparticles into the polysaccharides matrix. The morphology of nickel sulphides and

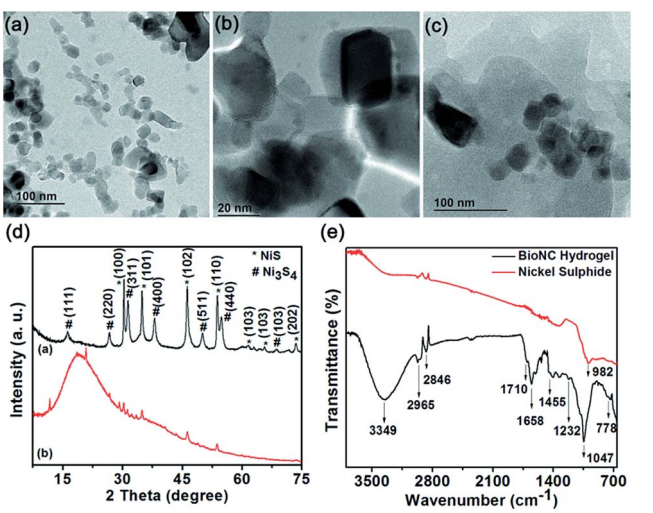


Fig. 1 TEM images of (a and b) nickel sulphide nanoparticles and (c) BioNC hydrogel nanocomposite; (d) XRD patterns of nickel sulphide nanoparticles (a) and BioNC hydrogel (b); (e) FT-IR spectra of nickel sulphide nanoparticles and nanocomposite.

BioNC hydrogel were observed, as typically shown in Fig. 1a–c. The TEM images show that NiS/$Ni_3S_4$ NPs consist of agglomerated spherical and nanorods structures (Fig. 1a and b). Agglomerated nanorods and spherical NiS/$Ni_3S_4$ NPs were also noticed in the TEM image of BioNC hydrogel (Fig. 1c) which confirmed that nanoparticles are well incorporated in the polysaccharides matrix Gk-cl-PAAm.

The SEM images of the Gk-cl-PAAm and BioNC hydrogel are shown in Fig. 2. The SEM image of the Gk shows a smooth surface (Fig. 2a), whereas the surface of the hydrogel polymers is relatively heterogeneous because of the cross-linking among different polymeric chains (Fig. 2b). The surface of the hydrogel polymer again became smooth after the incorporation of nanoparticles in the hydrogel polymer matrix which introduced homogeneity in the polymer (Fig. 2c). Moreover, the EDS spectrum of the BioNC hydrogel showed the peaks of Ni and S, which also confirms the successful incorporation of NiS/$Ni_3S_4$ nanoparticles in the hydrogel polymer matrix (Fig. 2d). Furthermore, the EDS mapping of the BioNC hydrogel showed the uniform distribution of the NiS/$Ni_3S_4$ NPs in the polymer matrix (Fig. 2e–h).

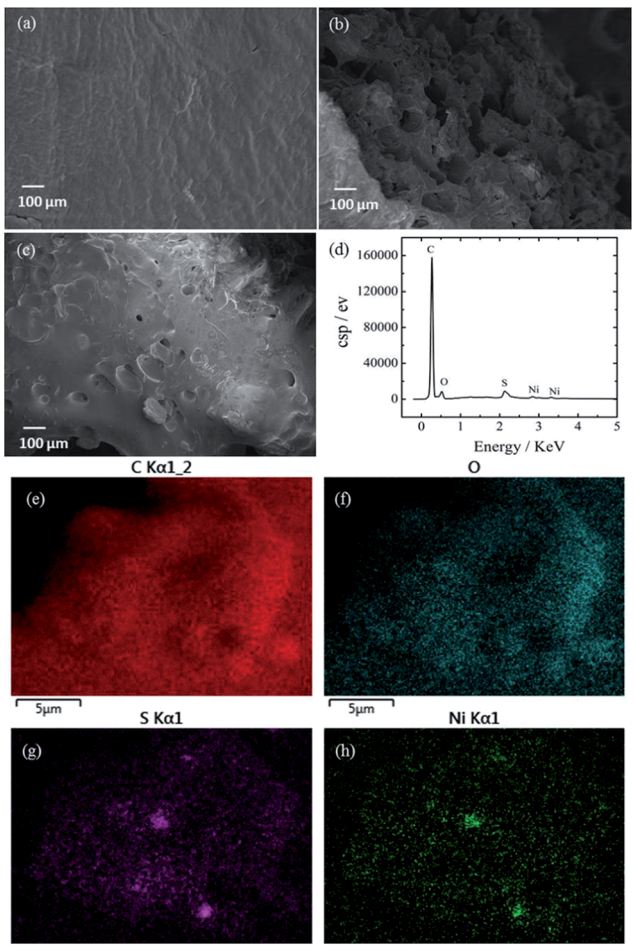


Fig. 2 SEM images of Gk (a), Gk-cl-PAAm (b) and BioNC hydrogel nanocomposites (c); (d) EDS spectrum and EDS mapping (e–h) of BioNC hydrogel nanocomposites.

BET studies were performed to observe the effects of the incorporation of NiS/$Ni_3S_4$ NPs on the surface area and pore volume of Gk-cl-PAAm hydrogel. The BET surface area, pore volume and pore diameter of Gk-cl-PAAm were 0.5215 $m^2\ g^{-1}$, 0.002356 $cm^3\ g^{-1}$ and 181.186 Å, respectively, which increased to 1.0284 $m^2\ g^{-1}$, 0.006654 $cm^3\ g^{-1}$ and 214.587 Å, respectively after the incorporation of NiS/$Ni_3S_4$ NPs in the Gk-cl-PAAm hydrogel. The concentration of –OH and –COOH functional groups available for the adsorption on the BioNC hydrogel was determined using the Boehm titration and it was found to be 0.052 meq $g^{-1}$ for the –COOH group and 0.0315 meq $g^{-1}$ for the –OH group.

## Adsorption studies

**Optimization of different adsorption parameters.** The adsorbent dose optimization is important to reduce the overall cost of the adsorption process and study the interactions of the adsorbate with the binding site of the adsorbent. A good adsorbent should be able to remove large amount of adsorbate from the aqueous solution with a low adsorbent dose and should be cost effective. The effect of the adsorbent dose on the percentage adsorption for R6G onto the BioNC hydrogel was studied at room temperature and neutral pH with different adsorbent doses of 0.1–0.6 g $L^{-1}$ in 50 mg $L^{-1}$ dye solutions (Fig. 3a). In the beginning, the percentage adsorption increased with increasing mass of the BioNC hydrogel. A possible reason is the increased number of adsorption sites with increased adsorbent dose, but further increase in the mass of the adsorbent did not significantly change the percentage adsorption.[35,37] The maximum 98% removal of R6G was observed with 0.4 g $L^{-1}$ adsorbent dose.

It is well known that the solution pH significantly affects dye removal with different adsorbent. Generally, the pH of the dye

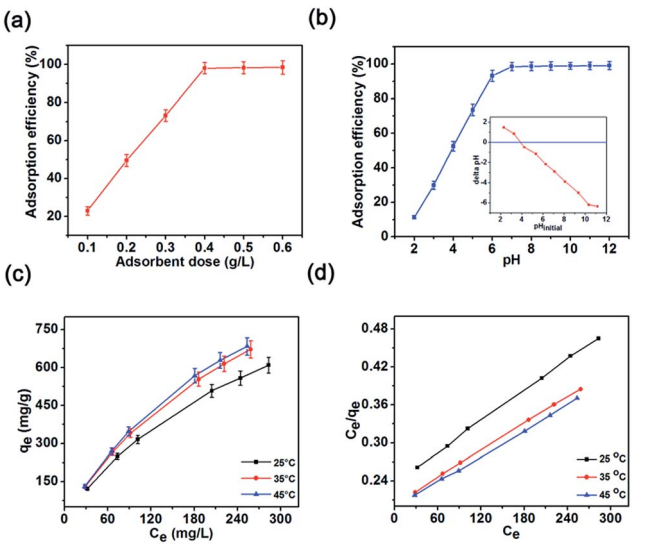


Fig. 3 Effect of the (a) polymer dose and (b) pH on the adsorption efficiency. Inset (b) plot of ΔpH *vs.* original pH for the calculation of pzc; plots for the (c) adsorption isotherm and (d) Langmuir isotherm for the adsorption R6G onto BioNC hydrogel nanocomposite.

solution exerts a profound impact on the adsorption sites of the adsorbent and ionization process of dye molecules. It has been observed that the percentage adsorption increases with increasing solution pH (Fig. 3b). This increase occurs because more adsorption sites are available. It was observed that the adsorption of cationic dyes follow the ionic mechanism, which mainly depends upon the type of interactions between the binding sites of the adsorbent and adsorbate molecules.[36,37] Therefore, the exact mechanism of the adsorption can be predicted based on the point zero charge (pzc) on the adsorbent surface. The adsorption of cationic dyes on the surface of any solid substrate is favourable at pH > pzc, whereas the adsorption of anionic dyes is favourable if pH < pzc. The pzc of the BioNC hydrogel was 3.83 (inset of Fig. 3b). Therefore, in the solutions of strongly acidic pH, the percentage adsorption was notably low, whereas the percentage adsorption increased with increasing solution pH. The lower percentage adsorption at highly acidic pH can also be attributed to the competitive adsorption of dye molecules with $H^+$ ions because the concentration of $H^+$ ions is notably high in strong acidic solutions. The BioNC hydrogel have most anionic binding site; therefore, $H^+$ ions in an acidic solution compete with cationic dye R6G molecules to interact with anionic binding sites and consequently decrease the adsorption percentage. The maximum adsorption (98%) was observed in a dye solution with initial pH of 6.5 and no noticeable change was subsequently found in the percentage adsorption. The pH effect on the adsorption of R6G has been well studied. Similar results were previously noticed for the solution pH effect on the adsorption of basic dyes such as methylene blue,[38] methyl green[39] and rhodamine B.[40] Because higher adsorption was obtained in the pH range of 6.5–11, the remainder of the batch experiments were performed at neutral pH. It is noteworthy that the possibility of maximum dye adsorption using the BioNC hydrogel without alteration of the solution pH, shows a practical application of the adsorbent.

The variation in the solution pH during the adsorption experiments was studied in the dye solution of initial pH = 7.0 for 4 h. It was observed that the solution pH decreased with the passage of time. In the first 75 min, the solution pH changed from neutral to 4.05 and then attained a constant value of 3.84 after 120 min (Fig. S1, ESI†). The solution pH decreased due to the release of $H^+$ ions present in the acidic and hydroxide groups of the backbone polymer.

**Adsorption isotherm.** The adsorption isotherm represents the interaction of the adsorbent with the adsorbate at constant temperature and the feasibility of a different adsorption process to adsorb a particular adsorbate. It also indicates the distribution of adsorption molecules between liquid and solid phase when the state of equilibrium is attained. The adsorption isotherm studies of R6G onto the BioNC hydrogel are conducted at three different temperatures: 25, 35 and 45 °C (Fig. 3c). The adsorption process in this study was endothermic because the adsorption of dye molecules increased with increasing temperature from 25 °C to 45 °C. In addition, the adsorption of dye molecules at all temperatures linearly increased with the increased initial dye concentration and saturated at higher initial dye concentrations. A possible reason is: the adsorbent has a fixed number of binding sites, which are sufficient for the adsorption of dye molecules at low initial concentrations, whereas in the solutions of high initial dye concentration, all the binding sites of the adsorbent were quickly occupied, and the surfaces became saturated, which caused adsorption equilibrium.[40] Therefore, in the solutions of higher initial dye concentration, less dye was removed. The experimental adsorption isotherm data were applied to the most frequently used adsorption isotherm models such as Langmuir (Fig. 3d), Freundlich (Fig. S2a, ESI†), Temkin (Fig. S2b, ESI†) and Dubinin–Kaganer–Radushkevich (DKR) (Fig. S2c, ESI†). Different isotherm parameters that were calculated using the aforementioned adsorption isotherms are provided in Table 1. The best adsorption model for the adsorption of R6G onto the BioNC hydrogel was applied based on the correlation coefficient $R^2$. By comparing the values of $R^2$ of adsorption isotherm models, it was observed that the Langmuir adsorption isotherm model was best fitted in this case (Table 1).

Langmuir isotherm is applicable for the monolayer adsorption and can be mathematically represented as follows:[26]

$$q_e = \frac{bq_m C_e}{1 + bC_e} \quad (6)$$

where, $b$ is Langmuir constant related to the adsorption free energy and affinity of adsorption (L $mg^{-1}$), $q_e$ is the amount of adsorbed dye at equilibrium (mg $g^{-1}$) and $q_m$ is the maximum adsorption capacity (mg $g^{-1}$) of the adsorbent. Further, Langmuir equation can be rearranged into a linearized form to calculate different Langmuir constants:[41]

$$\frac{C_e}{q_e} = \frac{1}{q_m b} + \frac{C_e}{q_m} \quad (7)$$

The values of Langmuir constants ($q_m$, $b$) were calculated from the slope and intercept of a linear plot between $C_e/q_e$ and $C_e$. Essential features and the applicability of Langmuir

Table 1 Isotherm parameters for the adsorption of R6G onto the BioNC hydrogel

| Isotherms | Isotherm constants | 25 °C | 35 °C | 45 °C |
|---|---|---|---|---|
| Langmuir | $q_m$ (mg $g^{-1}$) | 1244.71 | 1411.632 | 1477.10 |
| | $b \times 10^{-3}$ | 3.397 | 3.488 | 3.428 |
| | $R^2$ | 0.999 | 0.999 | 0.999 |
| | $R_L$ | 0.358–0.789 | 0.352–0.779 | 0.356–0.782 |
| Freundlich | $1/n$ | 0.729 | 0.744 | 0.753 |
| | $K_F$ | 10.308 | 11.200 | 11.074 |
| | $R^2$ | 0.993 | 0.994 | 0.992 |
| | $B$ | 227.59 | 252.298 | 260.0 |
| Temkin | $K_t$ | 21.705 | 20.258 | 20.161 |
| | $R^2$ | 0.973 | 0.970 | 0.972 |
| | $\beta$ | 8.410 | 6.750 | 6.145 |
| Dubinin–Kaganer–Radushkevich (DKR) | $q_D$ (mg $g^{-1}$) | 595.85 | 657.53 | 674.51 |
| | $E$ (kJ $mol^{-1}$) | 0.243 | 0.272 | 0.285 |
| | $R^2$ | 0.924 | 0.931 | 0.741 |

equation can be predicted by the following dimensionless constant, which is generally known as the separation factor ($R_L$).

$$R_L = \frac{1}{1 + bC_o} \quad (8)$$

where, $C_o$ is the initial concentration of R6G dye in solution (mg $L^{-1}$). There is a favourable value of $R_L$ between zero and one ($0 < R_L < 1$). If this value is greater than one, the isotherm is unfavourable ($R_L > 1$). If $R_L = 1$, then linear isotherm is obtained and if $R_L = 0$, the irreversible isotherm appears.[42] Experimentally, the values of $R_L$ are less than one for all three temperatures, which confirms the applicability of Langmuir adsorption isotherm model (Table 1). The calculated values of different Langmuir constants and correlation coefficients ($R^2$) are shown in Table 1. The constant correlation coefficient value (0.999) was found with maximum adsorption capacity of 1244.71, 1411.663 and 1477.10 mg $g^{-1}$ at 25 °C, 35 °C and 45 °C, respectively.

The high value of $R^2$ at all three temperatures showed a better fit of the Langmuir adsorption isotherm for the adsorption of R6G onto BioNC hydrogel (Table 1). Moreover, the increased value of Langmuir constant ($b$) with increasing temperature suggested the strong desirability of adsorbate molecules by the binding sites on the adsorbent surface and higher affinity between the adsorbate and adsorbent at higher temperatures than at lower temperatures. Therefore, from the applicability of Langmuir isotherm model it can be predicted that the adsorption of R6G on the surface of the BioNC hydrogel follows the homogeneous monolayer adsorption. It was also observed DKR isotherm model and Langmuir isotherm model provided different mean adsorption capacities ($q_D$) (Table 1) because of different assumptions in the formulation of these isotherm models. The reciprocal of heterogeneity factor *i.e.*, $1/n$ in Freundlich isotherm was less than unity for all studied temperatures which suggests that the adsorption of R6G onto the surface of the BioNC hydrogel is favourable in the entire studied range of concentrations of R6G solutions.[39] In the case of Temkin adsorption isotherm, $\beta$ increased with temperature (Table 1), which also supports the increase in adsorption capacity with the corresponding increase in temperature.[26]

Moreover, the type of adsorption process, *i.e.*, physical adsorption or chemisorptions can be predicted based on the apparent energy $E$, which is calculated using DKR. For any adsorption process to be physical adsorption, the value of $E$ should be less than 8.0 kJ $mol^{-1}$, whereas for chemisorption, it should be between 8.0 and 16.0 kJ $mol^{-1}$ (ref. 43) and for the adsorption of R6G onto the BioNC hydrogel, $E$ was observed to be less than 8.0 kJ $mol^{-1}$ for all three studied temperatures (Table 1). Therefore, it can be suggested that the adsorption of R6G onto the BioNC hydrogel was a physical adsorption process.

**Thermodynamic parameters.** The van't Hoff equation was used to find the spontaneity of the adsorption of R6G onto the hydrogel nanocomposite and to calculate various other thermodynamic parameters.[20,26]

$$\ln K_L = \frac{\Delta S^\circ}{R} + \frac{-\Delta H^\circ}{RT} \quad (9)$$

$$\Delta G^\circ = -RT \ln K_L \quad (10)$$

$$K_L = m\frac{q_e}{C_e} \quad (11)$$

where, $\Delta G^\circ$ is the change in Gibbs free energy (J $mol^{-1}$), $\Delta H^\circ$ is the change in enthalpy (J $mol^{-1}$), $\Delta S^\circ$ is the change in entropy (J $mol^{-1}$ $K^{-1}$), $q_e$ is the amount of adsorbed dye per unit mass of adsorbent (mg $g^{-1}$), $C_e$ is the equilibrium concentration (mg $L^{-1}$) of dye that remained in the solution after adsorption, $K_L$ is the distribution coefficient, $m$ is the adsorbent concentration (g $L^{-1}$), $T$ is the absolute temperature (K), and $R$ is the universal gas constant (8.314 J $K^{-1}$ $mol^{-1}$).

The values of $\Delta H^\circ$ and $\Delta S^\circ$ were evaluated from the slope and intercept of the linear plot of $\ln K_L$ *vs.* $1/T$ respectively (Fig. S3, ESI†). Eqn (10) was used to calculate the change in free energy ($\Delta G^\circ$). The calculated values of different thermodynamic parameters are shown in Table S2, ESI.† The positive values $\Delta S^\circ$ suggest an increase in disorder and randomness at the solid–liquid interfaces during the adsorption process and a positive value of $\Delta H^\circ$ indicates that the process is endothermic in nature.[43] However, $\Delta G^\circ$ decreased with increasing temperatures and signifies the spontaneous nature of R6G adsorption onto the BioNC hydrogel.[13]

**Adsorption kinetics.** The kinetics of adsorption depends on the interaction of solid–liquid interfaces and diffusion process.[45] The adsorption kinetics for the adsorption of R6B onto the BioNC hydrogel was studied in the dye solutions of three different initial concentrations (50, 75 and 100 mg $L^{-1}$), and the results are shown in Fig. 4a. The time required to reach adsorption equilibrium is inversely proportional to the initial dye concentration. The solution with lower initial dye concentration notably quickly reached adsorption equilibrium notably fast compared to the solutions with relatively higher initial dye concentration. A possible reason is the presence of strong adsorption driving forces in the solutions with lower initial dye concentration compared to those with higher initial dye concentrations.[37] Different kinetics models such as pseudo first-order (Fig. S4a, ESI†), pseudo second-order (Fig. 4b), Elovich (Fig. S4b, ESI†) and intra-particle diffusion models (Fig. 4c) were studied to evaluate the rate of adsorption and understand the adsorption mechanism. All kinetic parameters for the adsorption of R6G onto the BioNC hydrogel are summarized in Table 2.

The best adsorption kinetics model was decided by the value of $R^2$ and the pseudo second-order fitted the adsorption of R6B onto the BioNC hydrogel much better than the other adsorption kinetics modes.

The integrated mathematical form of the pseudo second-order rate equation is expressed as follows:[41]

$$\frac{t}{q_t} = \frac{1}{K_2 q_e^2} + \frac{t}{q_e} \quad (12)$$

where, $q_e$ (mg $g^{-1}$) and $q_t$ (mg $g^{-1}$) are the amounts of adsorbed dye per unit mass of adsorbate at equilibrium and time $t$, respectively; $k_2$ (g $mg^{-1}$ $min^{-1}$) is the pseudo second-order adsorption rate constant. $k_2$ was obtained from the slope and intercept of the plot of $t/q$ *versus* $t$, (Fig. 4b). All calculated and

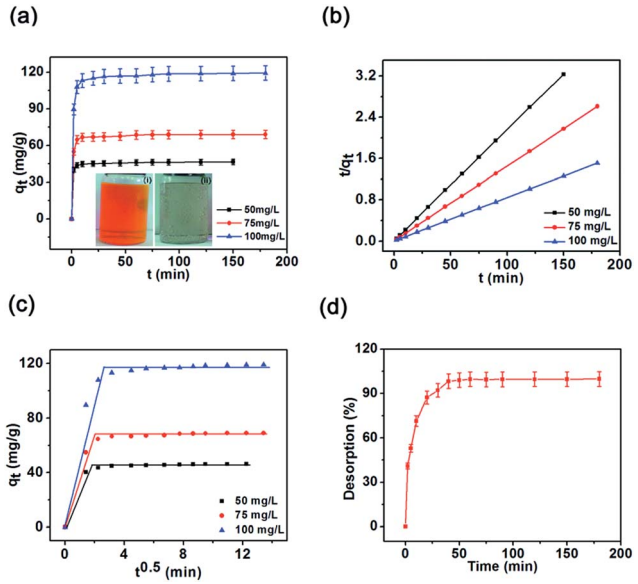


Fig. 4 Plots of the (a) adsorption kinetics, (b) pseudo-second-order model and (c) intraparticle diffusion model for the adsorption of R6G onto the BioNC hydrogel nanocomposite; (d) kinetics of desorption of R6G from R6G-loaded-BioNC hydrogel in 0.1 M HCl acid solution; inset photograph (a) of 100 mg $L^{-1}$ R6G dye adsorbed by hydrogel initially (i) and after 2 h (ii).

experimental values of different constants in the pseudo second order rate model are provided in Table 2.

The calculated values of $q_e$ using the pseudo second-order rate equation and experimental value of $q_e$ were almost similar, whereas the calculated values of $q_e$ using the pseudo-first-order rate equation significantly differs from the experimental value of $q_e$. Furthermore, the obtained values of $R^2$ using the pseudo second-order rate equation were much higher than the value of the pseudo-first-order equation (Table 2). Therefore, the mechanism of the adsorption of R6B onto the BioNC hydrogel can be better described using the pseudo second-order rate equation.

Table 2 Kinetic parameters for the adsorption of R6G onto the BioNC hydrogel nanocomposite

| Kinetic model | Kinetic parameters | 50 mg $L^{-1}$ | 75 mg $L^{-1}$ | 100 mg $L^{-1}$ |
|---|---|---|---|---|
| Pseudo first order | $k_1$ | 0.034 | 0.048 | 0.0322 |
| | $q_e$ (cal.) | 5.140 | 10.641 | 16.368 |
| | $q_e$ (exp.) | 46.44 | 68.75 | 119.22 |
| | $R^2$ | 0.699 | 0.908 | 0.785 |
| Pseudo second order | $k_2$ | 0.036 | 0.021 | 0.011 |
| | $q_e$ (cal.) | 47.61 | 71.42 | 119.61 |
| | $q_e$ (exp.) | 46.44 | 68.75 | 119.22 |
| | $R^2$ | 0.999 | 0.999 | 0.999 |
| Elovich | $\beta \times 10^{-2}$ | 82.713 | 41.89 | 19.398 |
| | $R^2$ | 0.826 | 0.693 | 0.730 |
| Intraparticle diffusion | $k_i$ | 14.276 | 21.46 | 36.475 |
| | $C_i$ | 7.836 | 9.96 | 15.52 |
| | $R^2$ | 0.791 | 0.838 | 0.860 |

The steps that determine rate of the adsorption process can be best described by the intraparticle diffusion model. This rate model is express as follows:[26]

$$q_t = k_i t^{0.5} + C \quad (13)$$

where, $q_t$ (mg $g^{-1}$) is the adsorption capacity at time $t$, and $k_i$ (mg $g^{-1}$ $min^{-0.5}$) is the rate constant. Plots of $q_t$ *versus* $t^{0.5}$ for all three concentrations were studied (Fig. 4c). The graphs did not pass through the origin with a straight line, and notably poor values of correlations coefficients were observed, which indicated that the intraparticle diffusion was not the rate limiting step for the adsorption of R6G onto the BioNC hydrogel.

**Comparison of the adsorption capacity of the BioNC hydrogel nanocomposites with other adsorbents.** The maximum adsorption capacity of the BioNC hydrogel for the adsorption of R6G was compared with other adsorbents and showed much better adsorption efficiency than some reported adsorbents (Table 3). Therefore, the BioNC hydrogel can be used as a potential adsorbent to adsorb cationic dyes such as R6G from the aqueous solution.

**Comparison of the adsorption efficiency of the BioNC hydrogel with parental polysaccharide matrix of Gk-cl-PAAm.** The adsorption efficiency of the BioNC hydrogel for the adsorption of R6G was compared with the parental polymer matrix *i.e.* Gk-cl-PAAm and the NiS/$Ni_3S_4$ NPs. The adsorption experiments were performed with dye solutions of different concentrations (100–500 mg $L^{-1}$) at 25 °C and the experimental data were fitted using the Langmuir adsorption isotherm (Fig. S5, ESI†). The maximum adsorption of the parental hydrogel polymer (*i.e.* Gk-cl-PAAm) was 357.17 mg $g^{-1}$, whereas for the NiS/$Ni_3S_4$ NPs it was found to be 263.15 mg $g^{-1}$ (Table S3, ESI†) which is considerably less than that of the hydrogel nanocomposites. The enhanced adsorption efficiency of the hydrogel nanocomposites to the parental hydrogel polymer as well as the NPs is attributed to the increased surface area, porosity, hydrodynamic volume and additional chelating binding sites on the surface because of the presence of nanoparticles.

**Adsorption of dyes from simulated wastewater.** It was observed that the adsorption efficiency of the BioNC hydrogel for all the dyes increased with increased polymer dose. In addition, the adsorbent showed much better adsorption performance for the adsorption of cationic dyes *viz.* methylene blue (MB), R6G, and brilliant green (BG) and an anionic dye Congo red (CR) (Fig. S6, ESI†). The better adsorption behaviour for the cationic dyes will be due to the presence of the various anionic functionalities on the surface of the BioNC hydrogel.

**Regeneration and reusability studies.** The regeneration and reusability of a particular type of adsorbents completely depend on its adsorption–desorption characteristics. Better reusability of the adsorbate is always in demand because of its economic viability, which strengthens the practical utility for potential large-scale applications. Therefore, the study of adsorption–desorption experiments for the regeneration of binding sites and reusability of adsorbent are necessary. Adsorption–desorption experiments were performed using 0.1 M HCl for 5

 

Table 3 Adsorption capacity comparison of the prepared bionanocomposite hydrogel in this study with other adsorbents to remove R6G

| Adsorbents | $q_m$ (mg g$^{-1}$) | pH | Dose (g L$^{-1}$) | Isotherm | Kinetics model | Reference |
|---|---|---|---|---|---|---|
| Activated carbon | 44.7 | 7 | 0.02 | Langmuir | Intraparticle diffusion | 46 |
| Hexadecyl functionalized magnetic silica nanoparticles | 35.6 | 11 | 0.30 | Langmuir | Pseudo-second-order | 47 |
| Palm shell powder | 105.0 | 5.75 | 0.40 | Langmuir | Pseudo-second-order | 48 |
| Titanium phosphate | 217.39 | 6 | 10 | Langmuir | — | 49 |
| Chitosan clay nanocomposite | 440.90 | 9 | 0.09 | Freundlich | Pseudo-second-order | 50 |
| Graphene–sand | 55 | — | 0.005 | — | Pseudo-second-order | 51 |
| Chitosan-*g*-(*N*-vinyl pyrrolidone)/ montmorillonite hydrogel | 36.6 | 10 | 0.05 | Freundlich | Pseudo-second-order | 52 |
| Graphene oxide | 23.3 | — | — | Langmuir | — | 32 |
| Almond shell (*Prunusdulcis*) | 32.6 | 8 | 10 | Langmuir | Pseudo-second-order | 53 |
| *Trichoderma harzianum* mycelial biomass | 3.40 | 8 | 20 | Langmuir | Pseudo-second-order | 54 |
| Exhausted coffee ground | 17.37 | — | 1 | Langmuir | Pseudo-second-order | 55 |
| Biological sludge | 16.3 | 7 | 10 | — | Pseudo-second-order | 56 |
| BioNC hydrogel | 1244.71 | 7 | 0.40 | Langmuir | Pseudo-second-order | This study |

successive cycles of adsorption and desorption. Furthermore, a kinetic study of the desorption process was conducted. The desorption process attained equilibrium in 60 minutes (Fig. 4d). No change in dye adsorption capacity was observed for the first three cycles, but a notably small reduction in adsorption capacity was noticed in the last two cycles (Fig. 5a). A similar adsorption–desorption behaviour of a different adsorbent for various dyes is well reported in the literature.[20,45,50] Therefore, these adsorption–desorption studies suggests that the BioNC hydrogel can be regenerated and reused to successively adsorb R6G for three times.

**Adsorption mechanism.** The adsorption efficiency of the adsorbents was determined using various parameters: numbers of active sites on the adsorbent surface, structural and functional behaviour of the adsorbate, surface characteristic of the adsorbent, mass transport process, dye diffusion process and interaction between adsorbate and adsorbent.[44,45,57] Here, the cationic dye R6G can be rapidly adsorbed on the anionic surface of the BioNC hydrogel because of van der Waals force, hydrogen bonding and electrostatic interactions.[57]

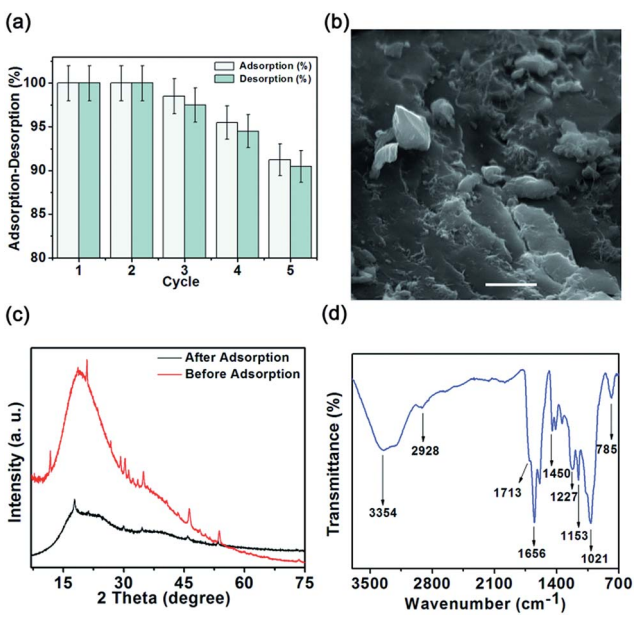


Fig. 5 (a) Performance of the BioNC hydrogel in multiple cycles of regeneration; characterisation of the BioNC hydrogel after the adsorption of R6G using (b) SEM, (c) XRD and (d) FT-IR techniques. The scale bar of the SEM image is 5 μm.

The possible interaction sites between hydrogel and dye molecules are shown in the FT-IR spectra of BioNC hydrogel (Fig. 1d) and R6G-dye-loaded BioNC hydrogel (Fig. 5d). Compared with the pure BioNC hydrogel, the characteristic peaks of the dye-loaded BioNC hydrogel are broadened and slightly shifted. For example, the –OH/–NH stretching vibration is broadened and shifted from 3349 to 3362 cm$^{-1}$, the COO$^-$ stretching vibration shifts from 1710 to 1716 cm$^{-1}$, the amide stretching vibration shifts from 1658 to 1651 cm$^{-1}$, the COO$^-$ asymmetric stretching vibration shifts from 1565 to 1590 cm$^{-1}$, the –NH in-plane bending vibration shifts from 1455 to 1456 cm$^{-1}$, and the amide –C–N stretching vibration shifts from 1232 to 1218 cm$^{-1}$. In addition, a new peak appears at 1153 cm$^{-1}$, which corresponds to –COC– of R6G, and indicates notably high adsorption of the dye onto the BioNC hydrogel. However, no significant change occurred for the –CH stretching vibration, *i.e.*, the peak at 2947 cm$^{-1}$. These changes indicate the specific electrostatic and hydrogen bonding interaction (Yoshida and dipole–dipole H-bonding) among the functional groups of dye molecules and hydroxyls, amides, carbonyl, –COO$^-$ and nickel nanoparticles groups on the BioNC hydrogel as shown in Scheme 2.

The morphological features and surface characteristics of the dye-loaded BioNC hydrogel were studied using SEM measurement (Fig. 5b). The SEM image indicates that the surface of the BioNC hydrogel became relatively heterogeneous because of the layers, which resulted from the accumulation of big R6G dye molecules on the surface. This result is further confirmed by the XRD spectrum in Fig. 5c. Changes occurred in the amorphous region (broadening) of the BioNC hydrogel XRD because of the increase in the number of aromatic dye

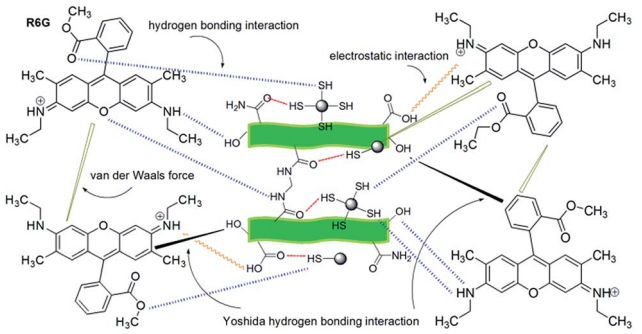


Scheme 2 Schematic diagram for the possible interactions between the BioNC hydrogel and R6G dye molecules.

molecules on the surface. The decrease in intensity of the characteristic peaks shows the occurrence of different interactions between dye molecules and BioNC hydrogel. Furthermore, the existence of an electrostatic interaction between the cationic dye molecules and the anionic adsorbent can be confirmed by the salt effect study, where the adsorption efficiency decreases with increasing ionic strength. The excellent regeneration property of the BioNC hydrogel reveals that the electrostatic interaction may be a main probable mechanism for the adsorption of cationic dye. Moreover, the adsorption efficiency and kinetics commonly depend on the number of available active sites, diffusion process and microstructure of the adsorbent.[57] Therefore, it is assumed that the rapid adsorption of cationic R6G dye mainly occurs because of the electrostatic interaction and hydrogen bonding interaction.

Overall, from the above mentioned adsorption studies, it can be concluded that the synthesized BioNC hydrogel have the potential to be used at the industrial scale. Moreover, the synthesized hydrogel nanocomposite is much more cost effective and economical as compared to the other commercially available adsorbents, such as activated carbon and zeolites, because the main component (more than 99%) of this material is synthesized using the gum polysaccharide which is an inexpensive highly abundant polymer.

## 4 Conclusions

From the aforementioned studies it can be concluded that the hydrogel nanocomposite of PAAm-grafted Gk and NiS/$Ni_3S_4$ NPs was successfully synthesized using the graft co-polymerization technique. Various morphological and structural characterization techniques proved the successful incorporation and homogeneous dispersion of the NiS/$Ni_3S_4$ NPs in the hydrogel polymer matrix. The adsorption of R6G (a cationic dye) followed the Langmuir monolayer adsorption model and pseudo second-order rate model with the maximum adsorption capacity of 1244.71 g $L^{-1}$. Thermodynamics studies show the endothermic and spontaneous nature of the adsorption process. Furthermore, the reusability experiments show that this adsorbent can be used for 3 successive cycles of adsorption–desorption. Therefore, these studies indicated that the BioNC hydrogel can be used as a potential adsorbent for the highly effective removal of cationic dyes from wastewater.

## Acknowledgements

Neeraj Kumar and Hemant Mittal are grateful to the National Research Foundation (NRF), South Africa and Faculty of Science, University of Johannesburg, South Africa for awarding the research fellowship.

## References

1 R. Gong, Y. Ding, M. Li, C. Yang, H. Liu and Y. Sun, *Dyes Pigm.*, 2005, **64**, 187.
2 C. Namasivayam and D. Sangeetha, *J. Hazard. Mater.*, 2006, **135**, 449.
3 T. Robinson, G. McMullan, R. Marchant and P. Nigam, *Bioresour. Technol.*, 2001, **77**, 247.
4 C. J. Ogugbue and T. Sawidis, *Biotechnol. Res. Int.*, 2011, **2011**, 967925.
5 Z. Wu and D. Zhao, *Chem. Commun.*, 2011, **47**, 3332.
6 Y. H. Li, S. Wang, J. Wei, X. Zhang, C. Xu, Z. Luan, D. Wu and B. Wei, *Chem. Phys. Lett.*, 2002, **357**, 263.
7 C. J. Madadrang, H. Y. Kim, G. Gao, N. Wang, J. Zhu, H. Feng, M. Gorring, M. L. Kasner and S. Hou, *ACS Appl. Mater. Interfaces*, 2012, **4**, 1186.
8 V. Gupta, *J. Environ. Manage.*, 2009, **90**, 2313.
9 N. Kumar, H. Mittal, L. Reddy, P. Nair, J. C. Ngila and V. Parashar, *RSC Adv.*, 2015, **5**, 38801.
10 V. K. Gupta and I. Ali, *Environ. Sci. Technol.*, 2008, **42**, 766.
11 I. Ali, *Chem. Rev.*, 2012, **112**, 5073.
12 H. Mittal, A. Maity and S. S. Ray, *Int. J. Biol. Macromol.*, 2015, **79**, 8.
13 H. Mittal, A. Maity and S. S. Ray, *J. Phys. Chem. B*, 2015, **119**, 2026.
14 S. A. N. Chakoli, J. He, M. A. Chayjan, Y. Huang and B. Zhang, *RSC Adv.*, 2015, **5**, 55544.
15 H. L. Parker, A. J. Hunt, V. L. Budarin, P. S. Shuttleworth, K. L. Miller and J. H. Clark, *RSC Adv.*, 2012, **2**, 8992.
16 K. Kabiri, H. Omidian, M. J. Zohuriaan-Mehr and S. Doroudiani, *Polym. Compos.*, 2011, **32**, 277.
17 A. Afkhami and R. Norooz-Asl, *Colloids Surf., A*, 2009, **346**, 52.
18 H. Mittal, R. Jindal, B. S. Kaith, A. Maity and S. S. Ray, *Carbohydr. Polym.*, 2014, **114**, 321.
19 M. U. Sankar, S. Aigal, S. M. Maliyekkal, A. Chaudhary, A. A. Kumar, K. Chaudhari and T. Pradeep, *Proc. Natl. Acad. Sci. U. S. A.*, 2013, **110**, 8459.
20 H. Mittal, A. Maity and S. S. Ray, *Chem. Eng. J.*, 2015, **279**, 166.
21 R. Rakhshaee and M. Panahandeh, *J. Hazard. Mater.*, 2011, **189**, 158.
22 H. Mittal and S. Mishra, *Carbohydr. Polym.*, 2014, **101**, 1255.
23 V. K. Gupta, S. Agarwal and T. A. Saleh, *Water Res.*, 2011, **45**, 2207.
24 J. Virkutyte, V. Jegatheesan and R. S. Varma, *Bioresour. Technol.*, 2012, **113**, 288.

 

25 Z. Yang, S. Chen, W. Hu, N. Yin, W. Zhang and C. Xiang, *Carbohydr. Polym.*, 2012, **88**, 173.
26 H. Mittal, V. Parashar, S. Mishra and A. Mishra, *Chem. Eng. J.*, 2014, **255**, 471.
27 B. Paul, V. Parashar and A. Mishra, *Environ. Sci.: Water Res. Technol.*, 2015, **1**, 77.
28 J. M. Falkowski, N. M. Concannon, B. Yan and Y. Surendranath, *J. Am. Chem. Soc.*, 2015, **137**, 7978.
29 E. L. Hirst and S. Dunstan, *J. Chem. Soc.*, 1953, 2332.
30 E. Fosso-Kankeu, H. Mittal, F. Waanders, I. O. Ntwampe and S. S. Ray, *Int. J. Environ. Sci. Technol.*, 2016, **13**, 711.
31 C. Moreno-Castilla, M. V. Lopez-Ramon and F. C. Marin, *Carbon*, 2000, **38**, 1995.
32 H. Ren, D. D. Kulkarni, R. Kodiyath, W. Xu, I. Choi and V. V. Tsukruk, *ACS Appl. Mater. Interfaces*, 2014, **6**, 2459.
33 N. A. Almuslet, E. A. Hassan, A. S. A.-El.-M. Al-Sherbini and M. G. A. Muhgoub, *Elixir Chem. Phys.*, 2011, **33**, 2227.
34 S. Pan, J. Zhu and X. Liu, *New J. Chem.*, 2013, **37**, 654.
35 L. Liu, Z. Y. Gao, X. P. Su, X. Chen, L. Jiang and J. M. Yao, *ACS Sustainable Chem. Eng.*, 2015, **3**, 432.
36 J. Wang, G. Zhao, Y. Li, H. Zhu, X. Peng and X. Gao, *Dalton Trans.*, 2014, **43**, 11637.
37 S. K. Dhanya, J. Joy and T. P. Rao, *Sens. Actuators, B*, 2012, **173**, 510.
38 C. L. Fan, M. Sun, X. Li, F. Luand and H. Qiu, *Bioresour. Technol.*, 2012, **114**, 703.
39 B. H. Hameed, *J. Hazard. Mater.*, 2008, **154**, 204.
40 H. Mittal, N. Ballav and S. Mishra, *J. Ind. Eng. Chem.*, 2014, **20**, 2184.
41 Z. Li, B. Yang, S. Zhang, B. Wang and B. Xue, *J. Mater. Chem. A*, 2014, **2**, 10202.
42 Y. Zhai, X. Wei, G. Zeng, D. Zhang and K. Chu, *Sep. Purif. Technol.*, 2004, **38**, 191.
43 T. A. Khan, S. Dahiya and I. Ali, *Appl. Clay Sci.*, 2012, **69**, 58.
44 R. S. Blackburn, *Environ. Sci. Technol.*, 2004, **38**, 4905.
45 S. Ghorai, A. Sarkar, M. Raoufi, A. B. Panda, H. Schönherr and S. Pal, *ACS Appl. Mater. Interfaces*, 2014, **6**, 4766.
46 G. Annadurai, R. S. Juang and D. J. Lee, *J. Environ. Sci. Health, Part A: Toxic/Hazard. Subst. Environ. Eng.*, 2001, **36**, 715.
47 C. Yan-Ping, C. Rena, Q. Yanga, Z. Y. Zhanga, L. J. Donga, C. Xing-Guo and X. De-Sheng, *Appl. Surf. Sci.*, 2011, **257**, 8610.
48 G. Sreelatha and P. Padmaja, *Am. J. Environ. Prot.*, 2008, **2**, 63.
49 K. C. Maheria and U. V. Chudasama, *Ind. Eng. Chem. Res.*, 2007, **46**, 6852.
50 A. Vanamudan and P. Pamidimukkala, *Int. J. Biol. Macromol.*, 2015, **74**, 127.
51 S. S. Gupta, T. S. Sreeprasad, S. M. Maliyekkal, S. K. Das and T. Pradeep, *ACS Appl. Mater. Interfaces*, 2012, **4**, 4156.
52 A. Vanamudan, K. Bandwala and P. Pamidimukkala, *Int. J. Biol. Macromol.*, 2014, **69**, 506.
53 H. B. Senturk, D. Ozdes and C. Duran, *Desalination*, 2010, **252**, 81.
54 S. Sadhasivam, S. Savitha and K. Swaminathan, *J. Environ. Manage.*, 2007, **85**, 155.
55 K. Shen and M. A. Gondal, *J. Saudi Chem. Soc.*, 2013, DOI: 10.1016/j.jscs.2013.11.005.
56 G. Annadurai, R. S. Juang, P. S. Yen and D. J. Lee, *Adv. Environ. Res.*, 2003, **7**, 739.
57 R. Gong, J. J. Ye, W. Dai, X. Y. Yan, J. Hu, X. Hu, S. Li and H. Huang, *Ind. Eng. Chem. Res.*, 2013, **52**, 14297.